Field-circuit coupled system simulation of a PMSM servo drive and comparison with measurements

Thomas Herold, Enno Lange and Kay Hameyer
Institute of Electrical Machines (IEM)
www.iem.rwth-aachen.de
RWTH Aachen University
Schinkelstraße 4, 52062 Aachen, Germany
Email: thomas.herold@iem.rwth-aachen.de

***Abstract*—While analytical descriptions of the electrical machine perform very well with respect to computational time giving acceptable results when compared to measurements, one may sacrifice the low computational effort in order to obtain more accurate results by including a Finite Element Analysis of the electrical machine. With this approach it is possible to study effects such as saturation and mutual influences in combination with the power electronics and the control. In this paper such a field-circuit coupled simulation of a PMSM servo drive is performed and the results are discussed. Furthermore, the different components are introduced and explained.**

***Index Terms*—circuit simulation, electromagnetic coupling, Finite Element Methods, permanent magnet machine, simulation**

I. Introduction

The simulation of electrical machines is a very important topic within many technical applications. On the one hand there are simulations performed for an optimal design. On the other hand control strategies are tested in simulation environments. The electromagnetic design process often bases on the Finite Element Analysis (FEA). This approach can help to design machines with high power density, a wide operating sector of high efficiency, and reduced noise [1], [2]. But the influences of the power electronics and circuit elements as well as the control strategy are not considered.
On the contrary, the control design for electrical machines rather uses an analytical approach and is tested within a block diagram oriented simulation environment (AS) e.g. Matlab/Simulink^{TM} [3], [4]. For this purpose a two axis model (d-q model) that represents the fundamental wave equations of the machine can be used. Certainly, this approach neglects some effects as nonlinearities, harmonics, mutual flux influences, and also the power electronics. To increase accuracy one can extend the model with parameters derived from FEA [5], [6]. Furthermore, a circuit simulator (CS) can be included for the simulation of the electrical circuit of the inverter. But even this modeling strategy remains an approximation that can be improved. A good approach for increasing the accuracy of both, the FEA and the AS/CS, is to combine them in an overall simulation. Several works about field-circuit coupling (FC) have been published in recent years. Two strategies have been investigated: The numerically strong coupling using the same time step for the FEA and the FC on the one hand and the numerically weak coupling that differs between two time step domains on the other hand. Since the energy and thus the parameters within the FEA are not changing as fast as e.g. the PWM signal of the power electronics it is reasonable to use the weak coupling with an elaborated time step mechanism saving significant computational effort.
In this paper a field-circuit coupled simulation of a PMSM servo drive is presented. The machine is represented by a Finite-Element model, the inverter is implemented within a circuit simulator, and the control uses a block diagram oriented simulation environment. In chapter II the simulation topology is shown and the different components are defined. After that two experiments, including the simulation and a corresponding measurement of a PMSM test-bench, are shown and compared in chapter III. Finally, the paper is concluded in chapter IV.

II. Simulation environment

Creating the simulation environment requires the different components to be modeled in their respective simulation domains. In the case of the examined servo drive these components are the machine, the control, and the inverter. The control is represented by an analytical description within the graphical simulation environment Simulink^{TM} solving ordinary differential equations (ODE). The inverter is modeled in the circuit simulation tool Plecs^{TM} while the numerical field computation is performed by the IEM in-house FEA software (www.iem.rwth-aachen.de). The fundamental platform for the overall simulation is based on Simulink as well. Fig. 1 shows an overview of the entire simulation environment. While the electrical and mechanical equations and the control are embedded in the analytical solver platform Simulink the circuit simulation and the FEA are additionally attached. These parts, i.e. the CS, the FEA, the electrical and mechanical equations together, and the trigger control, represent the field-circuit coupling (dashed box)(Fig. 1).
In the following the single components are enlarged and the parameter and signal exchange is explained.

A. Circuit Simulation

Within this simulation block the power electronics with the dc-link and the inverter are implemented. It receives the gate signals for the IGBTs from the control and delivers the terminal voltage to the electrical equations. The dc-link and the valves are modeled as ideal components. This means that the dc voltage is constant over the whole simulation period and that the generated terminal voltages are ideal rectangles. This does not have much impact to the simulation accuracy since

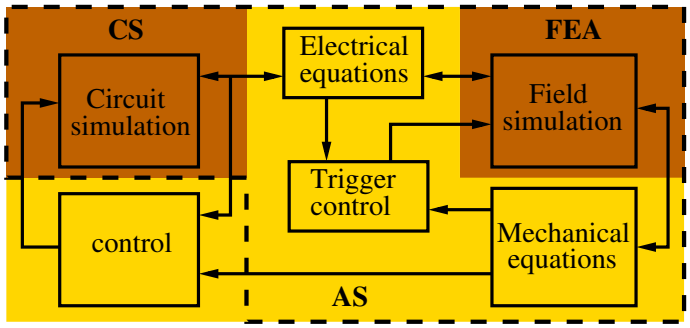

Fig. 1. The overall simulation environment.

the dc link voltage of the used inverter is controlled to a fix value which exceeds the semiconductor voltage drop by orders. Contrary to this idealization the IGBT timings are included to simulate the blanking time of the inverter which is to protect the inverter legs against a "shoot through". This blanking time causes a nonlinear relationship between the duty cycle and the average output voltage. For the accuracy of the overall simulation it is important to identify the dead-time of the used inverter. Therefore, two inverter legs are fed with a duty cycle of 50% whereas the third one is continuously increased from 0.35 to 0.65 within 15 s. With this slow increase an approximated steady-state motor current for each adjusted duty cycle is guaranteed. The result of this experiment (current vs. duty cycle) is shown in Fig. 2 (lower picture). It can be seen that there is a dead band between approx. $a_1 = 0.42$ and $a_2 = 0.58$. The blanking time can now be calculated by

$$T_d = \frac{\Delta V T}{2V_{DC}} = \frac{a_2 - a_1}{2} V_{DC} \frac{T}{2V_{DC}} = \frac{a_2 - a_1}{4} \cdot T \qquad (1)$$

with the voltage deviation ΔV , the dc-link voltage V_{DC}, and the length of one PWM cycle T [7]. For a PWM frequency of 8 kHz T_d is determined to 5 μs. The upper picture of Fig. 2 shows a simulation result with an included T_d. Although the measured current is more round shaped in the transition region the basic profile is reflected.

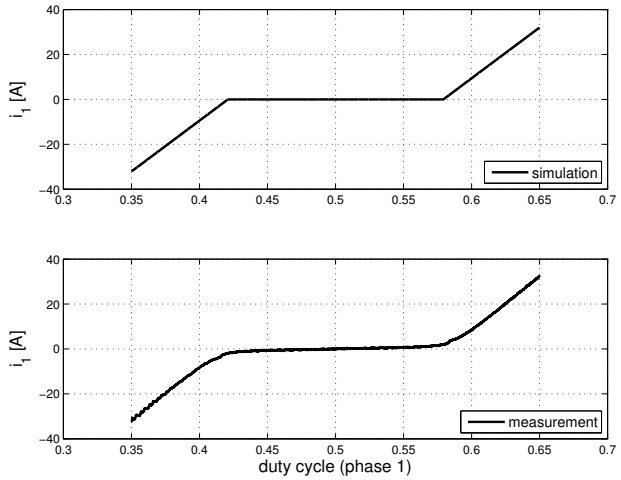

Fig. 2. Simulated and measured inverter dead-time behavior.

B. Lumped parameter extraction from FEA

Whenever the trigger control sends a signal, a new set of lumped parameters must be extracted from the FE model. For the device under test, a continuous evaluation of the energy flows of the electrical as well as the mechanical domain ensures a smooth extraction of the parameters, which is based on the balance of energy of the electrical machine, as presented in [8]. The three-phase PMSM is represented by an induction matrix L^{∂}_{kl} of self and mutual inductances with dimension 3x3 and a vector of motion induced voltages e_k with dimension three. The flux induced voltage of phase k is given by the time derivative of the flux linkage ψ_k (with implicit summation over l) as the difference of the terminal voltage v_k and the ohmic voltage drop Ri_k:

$$\partial_t \psi_k = v_k - Ri_k = \partial_t \psi_{kl} + \partial_t \psi_{f,k} \quad . \qquad (2)$$

Herein, $\psi_{f,k} = f(\alpha)$ is the remanence flux embraced by the permanent magnets being a function of the angular position of the rotor $\alpha = f(t)$, and $\psi_{kl} = f(\alpha, i_l)$ is the flux linkage in phase k depending on the current $i_l = f(t)$ carried by phase l and the rotor position α. Propagating the differential operator in (2), one yields:

$$\begin{aligned}
\partial_t \psi_k &= \partial_t (L_{kl} i_l) + \partial_t \psi_{f,k} \\
&= (\partial_t L_{kl})\, i_l + L_{kl}\, (\partial_t i_l) + \partial_t \psi_{f,k} \\
&= (\partial_t i_l \partial_{i_l} L_{kl})\, i_l + \omega\, (\partial_\alpha L_{kl})\, i_l + L_{kl}\, (\partial_t i_l) + \partial_t \psi_{f,k} \\
&= \partial_t i_l\, ((\partial_{i_l} L_{kl}) i_l + L_{kl}) + \omega (\partial_\alpha L_{kl}) i_l + \omega \partial_\alpha \psi_{f,k} \\
&= (\partial_t i_l)\, L^{\partial}_{kl} + \omega \partial_\alpha \psi_k = (\partial_t i_l)\, L^{\partial}_{kl} + \omega e^*_k \quad .
\end{aligned} \qquad (3)$$

The first term of (3) expresses the induced voltage by the flux linkage described by the inductance matrix L^{∂}_{kl} and the second term the motion induced voltage with the speed normalized electromotive force (emf) e^*_k. These parameters are given to the electrical equations where the corresponding line currents are calculated which are sent back to the field simulation afterwards.

C. Trigger control

The trigger control is an important aspect of the field-circuit coupled simulation. Herein, the time step of the FEA is determined. The implemented FC is based on the weak coupling implying different steps for the circuit simulations and the FEA. This may save a lot of computational effort since the time constant of the field domain τ_{FEA} usually exceeds the time constant of the circuit domain τ_{AS} by orders of magnitude and thus the relation for the time steps is $\Delta T_{FEA} >> \Delta T_{AS}$. The simplest approach for trigger generation is using a fixed step size. But if e.g. the currents are changing relatively fast, the lumped parameter representation of the machine would change significantly, especially if the machine operates in saturation. On the contrary, if the operating point is not or even slowly changing, an unnecessary, time consuming, extraction of a new set of lumped parameters may be forced.
A more reasonable approach is to adapt the time step. This can be done by energy considerations. Whenever the energy in the system is changing by a certain amount the trigger control enforces an extraction of a new set of lumped parameters from

the FEA. The energy in the system is subdivided in four parts, which are calculated as follows (with implicit summation over k).
The electrical energy is given by the terminal values v_k and i_k:

$$E_{elec} = \int v_k i_k \mathrm{d}t \quad . \tag{4}$$

The ohmic losses of the windings have to be considered as well:

$$E_{ohmic} = R \int i_k^2 \mathrm{d}t \quad . \tag{5}$$

The energy

$$E_{mag} = \frac{1}{2} i_k \psi_k = \frac{1}{2} i_k \int (v_k - R i_k - \omega e_k^*) \mathrm{d}t \tag{6}$$

represents the magnetic energy stored in the field of the machine's coils. The mechanical energy is calculated by rotational speed and torque:

$$E_{mech} = \int \omega T \mathrm{d}t \quad . \tag{7}$$

A new trigger signal is now generated at the time $t_1 > t_0$ of the last valid parameter extraction when the overall energy $E_{tot} = \sum E$ changes by a given specific threshold p, e.g. $p = 5\%$:

$$t_1 = t_0 + \Delta T_{FEA} \tag{8}$$

with

$$\Delta T_{FEA} = t|_{(e_{tot} \geq p)} - t_0 \tag{9}$$

and

$$e_{tot} = \frac{E_{tot}(t)}{E_{tot}(t_0)} \quad . \tag{10}$$

To ensure that position dependent influences are not neglected if the energy change remains below p, an additional trigger condition for the position is applied

$$\Delta T_{FEA} = t|_{(\Delta\alpha \geq \alpha_0)} - t_0 \tag{11}$$

where $\Delta\alpha = \alpha(t) - \alpha(t_0)$ is the change of the rotor position and α_0 a predefined difference angle. After a trigger signal has been sent the time t_0 is set to the new time t_1.
To get an idea of the computational effort: 1 s simulation means 5 min computational time with an analytical machine representation and 24 h with the numerical machine representation at weak coupling with $p = 0.05$ and $\alpha_0 = 2\,^\circ$.

D. Electrical and mechanical equations

Electrical equations: Two designs for the calculation the motor currents are feasible. The first one is the determination of the currents outside the CS generating a signal given to signal controlled current sources within the CS. The terminal voltages of the machine are the voltages over these current sources. The second design is the modeling of the motor inductance, resistance, and induced voltage directly within the CS. For this purpose the simulation software has to provide controllable mutual inductances.
For this work the first alternative is used. Therefore, the line

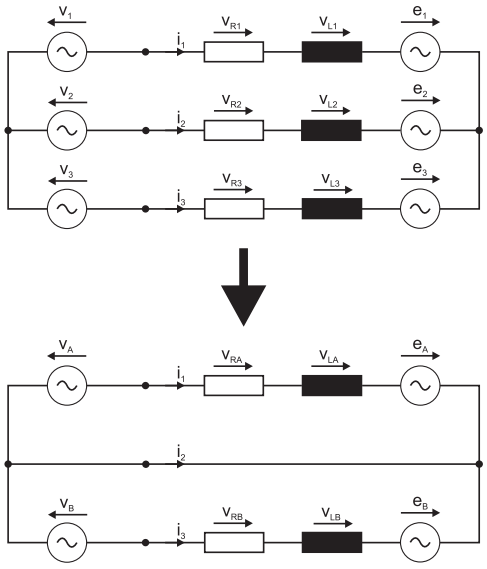

Fig. 3. Reducing of circuit elements to solve overdetermination.

currents of the machine are calculated by (2) and (3) after being transformed to

$$i = (L^\partial)^{-1} \int (v - Ri - \omega e^*) \mathrm{d}t \quad . \tag{12}$$

Since there is no zero phase-sequence system, the current equation above is overdetermined if solved independently for each phase. To solve this overdetermination the system is transformed as shown in Fig. 3. Now, only two phase currents are calculated whereas the third is given by Kirchhoff's law. This is implemented within the simulation block "Electrical equations". The currents are sent back to the circuit simulator's signal controlled current sources and given to the FEA as well. They can be written as

$$\begin{aligned} i_1 &= \int \frac{l_3}{l_1 l_3 - l_2 l_4} (A - \frac{l_2}{l_3} B) \mathrm{d}t \\ i_3 &= \int \frac{l_1}{l_1 l_3 - l_2 l_4} (B - \frac{l_1}{l_4} A) \mathrm{d}t \end{aligned} \tag{13}$$

with the abbreviations

$$\begin{aligned} A &:= v_1 - v_2 - e_1 + e_2 - R(2i_1 + i_3) \\ B &:= v_3 - v_2 - e_3 + e_2 - R(2i_3 + i_1) \\ l_1 &:= L_{11}^\partial - L_{21}^\partial - L_{12}^\partial + L_{22}^\partial \\ l_2 &:= L_{13}^\partial - L_{23}^\partial - L_{12}^\partial + L_{22}^\partial \\ l_3 &:= L_{33}^\partial - L_{23}^\partial - L_{32}^\partial + L_{22}^\partial \\ l_4 &:= L_{31}^\partial - L_{21}^\partial - L_{32}^\partial + L_{22}^\partial \quad . \end{aligned} \tag{14}$$

Mechanical equations: As aforementioned, the time steps of the FEA and the AS are different. Therefore, it is necessary to calculate the speed ω and position angle α of the machine outside the FEA to obtain a smooth curve. This is done by the mechanical equations

$$\begin{aligned} \omega &= \frac{1}{J} \int (T_{el} - T_{load} - T_{loss}) \mathrm{d}t \\ \alpha &= \int \omega \mathrm{d}t \end{aligned} \tag{15}$$

where J is the moment of inertia, T_{el} the electromagnetic torque of the machine, T_{load} the machine's load, and T_{loss} the speed dependent losses. The electrical torque is calculated by the FEA which in turn is fed by the phase currents and the rotor position α.

E. Control

Operating a PMSM servo commonly requires a closed loop control. Here, we use a PI cascade with an inner current and an outer speed control. The current control consists of two PI controllers responsible for the d- and the q-current respectively. They are designed as zero-pole compensation with a reduction of the effective time constant to a fifth of the natural one. To assist the controllers a subsequent static decoupling network compensating the axis cross-coupling and the induced voltage is added [9]. The speed control only consists of a proportional part to avoid overshoots leading to oscillation that will increase the experiment time since they have to be decayed for a steady-state analysis. The duty cycles for the PWM are generated by a space vector modulation (SVM) [10].

III. Experiment results

With the described simulation environment two experiments, including a simulation and a corresponding measurement, are performed and compared: a startup of a machine and a steady-state load scenario. The device under test is a PMSM servo coupled to a load machine. In Tab. I some data of the PMSM are given. The machine has an almost sinusoidal

Stator + cable resistance (measured)	R	$0.9\,\Omega$
Inductance (direct axis - data sheet)	L_d	0.6 mH
Inductance (quadrature axis - data sheet)	L_q	0.6 mH
Mass of inertia (overall drive train)	J	$2.69\,\mathrm{kgcm}^2$
Number of pole pairs	p	3
Nominal torque	T_N	8.4 Nm
Nominal current	I_N	9.3 A
Max. avg. tooth flux density (zero current-FEA)	B_{m0}	1.7 T

TABLE I
Data of the device under test.

induced voltage, only little position dependent inductance deviations, and a small cogging torque. Therefore, the influence of this parameters to the current waveform are negligible and thus the influence of the voltage switching semiconductors and the inverter dead time are good observable. Only the saturation of the machine has a significant influence to the experiments. In the area of operation of the experiments explained in this paper the saturation state of the machine is almost constant but the inductances are differing considerably to the ones given in the data sheet. This influence was investigated in a previous work [11].

A. Startup operation

For the startup the load machine is in no load condition that only the mass of inertia and the losses have to be compensated. For proper simulation conditions the losses basing on friction and eddy-currents are determined by measurements of the transferred torque at no-load. In Fig. 4 the machine's speed of the simulation and the measurement is shown. The

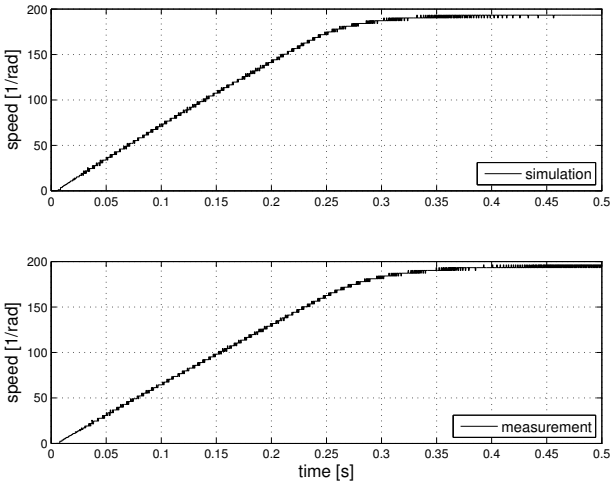

Fig. 4. Startup operation - speed.

quantization noise of the speed is caused by the incremental position encoder with a resolution of 4096 per turn, which is also simulated. However, this speed curves do not tell much about the quality of the simulation and a closer look to the stator currents is given in Fig. 5. Here, it can be seen that the startup operation within the simulation is faster than the measurement which bases on a minor difference in the mass of inertia or the developed torque. The effect of the inverter becomes visible in the current waveform that differ from an ideal sinusoidal shape.

B. Steady-state load operation

For a further investigation of the current waveforms an experiment with a steady-state load of $0.7 \cdot T_N$ is performed. The simulated and measured currents are shown in Fig. 6. Here, the harmonic distortion is clearly observable. A better impression about the harmonic content gives an FFT of the currents, shown in Fig. 7. For a better resolution of the harmonic frequencies the fundamental wave (≈ 9 A) is truncated. One can see the PWM influence at 4 and 8 kHz and some

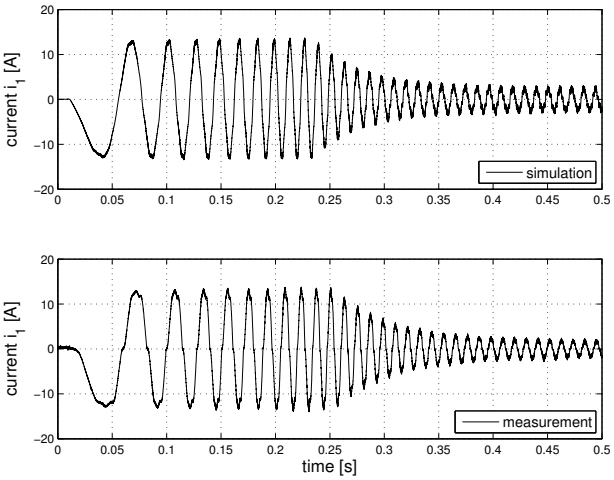

Fig. 5. Startup operation - currents.

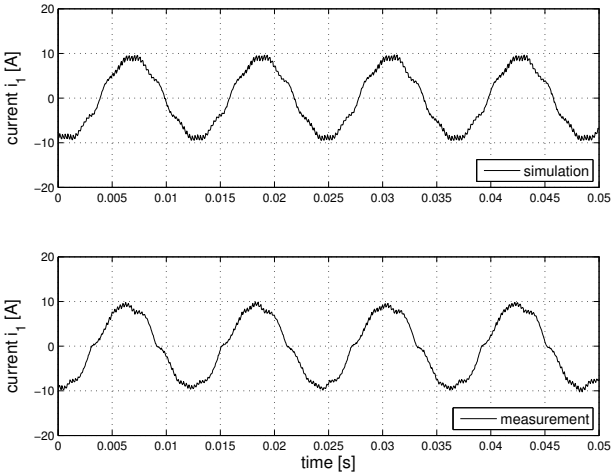

Fig. 6. Load operation - currents.

peaks below 2 kHz representing the 5th, 7th, 11th, 13th,.... harmonic that occur at operation with SVM and inverter deadtimes [12]. Although the frequencies are exactly reproduced by the simulation, the amplitudes of the harmonics show partially differences about $\approx 30\%$. This indicates that the modeling of the inverter is not sufficient yet. Moreover, the SVM dependent harmonics have a phase difference of $180\,^\circ$ which can be seen in the current plot. This also shows the inadequate inverter representation.

IV. Discussion and conclusions

In this paper a weak coupled field-circuit simulation of a PMSM servo is presented combining a circuit simulation for the power electronics, a numerical field simulation for the machine and a machine control. All different components are explained with the focus on the lumped parameter extraction of the FEA, the trigger control for an extraction of a new set of lumped parameters, and the prerequisites for coupling the FEA to the FC and AS. Furthermore, simulation results and measurements are presented and compared showing promising results. At first it can be summarized that the basic concept behind the presented field-circuit coupling is proven. A stable numerical simulation could be reached that shows a good correlation to measurement. Although the time characteristics (simulation and measurement) of the experiments are quite similar there are however notable deviations. At first the harmonic amplitudes are differing about $\approx$30%. Moreover, the inverter induced harmonics show different algebraic signs which also indicates a insufficient inverter modeling. Therefore, further investigations will focus on the power electronics to get a more precise representation on the one hand. On the other hand a machine with distinctive position depended inductances (e.g. a switched reluctance machine) will be investigated to get more information about the the accuracy of the field solution.

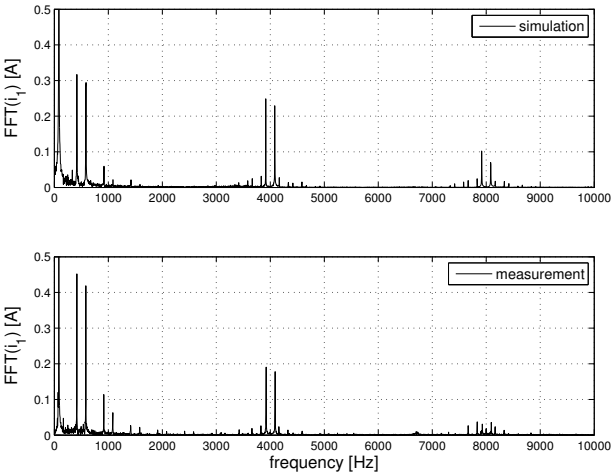

Fig. 7. Load operation - FFT analysis of currents.

References

[1] Chao-hui Zhao; Haihong Qin; Yang-guang Yan; , "Analysis of the Pole Numbers on Flux and Power Density of IPM Synchronous Machine," Power Electronics and Drives Systems, 2005. PEDS 2005. International Conference on , vol.2, pp.1402-1407.

[2] Franck, David; Hameyer, K.; , "Simulation of Acoustic Radiation of an AC Servo Drive Verified by Measurements," International Symposium on electromagnetic fields , ISEF 2009.

[3] Rujing Xiao; Xiangyu Yang; Wenjuan Zhu; Jianghua Cao; , "Modeling and simulation of dual-rotor permanent-magnet synchronous motor based on MATLAB," Electrical Machines and Systems, 2009. ICEMS 2009. International Conference on , pp.1-4, 15-18 Nov. 2009.

[4] Iyer, N.P.R.; Jianguo Zhu; , "Modeling and Simulation of A Six Step Discontinuous Current Mode Inverter Fed Permanent Magnet Synchronous Motor Drive Using SIMULINK," Power Electronics and Drives Systems, 2005. PEDS 2005. International Conference on , vol.2, pp. 1056- 1061, 28-01 Nov. 2005.

[5] Petkovska, L.; Cvetkovski, G.; , "FEM Based Simulation of a Permanent Magnet Synchronous Motor Performance Characteristics," Power Electronics and Motion Control Conference, 2006. IPEMC 2006. CES/IEEE 5th International , vol.1, pp.1-5, 14-16 Aug. 2006.

[6] Dempewolf, K.-H.; Ponick, B.; , "Modelling of permanent magnet synchronous machines for simulations of transient phenomena," Power Electronics and Applications, 2007 European Conference on , pp.1-10, 2-5 Sept. 2007.

[7] Seung-Gi Jeong; Min-Ho Park; , "The analysis and compensation of deadtime effects in PWM inverters ," Industrial Electronics, IEEE Transactions on , vol.38, no.2, pp.108-114, Apr 1991

[8] F. Henrotte and K. Hameyer, "The Structure of EM Energy Flows in Continuous Media," Magnetics, IEEE Transactions on, vol. 42, no. 4, pp. 903-906, April 2006.

[9] Hao Zhu; Xi Xiao; Yongdong Li; , "PI type dynamic decoupling control scheme for PMSM high speed operation," Applied Power Electronics Conference and Exposition (APEC), 2010 Twenty-Fifth Annual IEEE , vol., no., pp.1736-1739, 21-25 Feb. 2010

[10] van der Broeck, H.W.; Skudelny, H.-C.; Stanke, G.V., "Analysis and realization of a pulsewidth modulator based on voltage space vectors," Industry Applications, IEEE Transactions on , vol.24, no.1, pp.142-150, Jan/Feb 1988.

[11] Herold, Thomas; Lange, Enno; Hameyer, Kay; , "System simulation of a PMSM servo drive using the field-circuit coupling," Electromagnetic Field Computation (CEFC), 2010 14th Biennial IEEE Conference on , vol., no., pp.1-1, 9-12 May 2010

[12] Kaitwanidvilai, S.; Khan-Ngern, W.; Panarut, M.; , "The impact of deadtime effect on unwanted harmonics conducted emission of PWM inverters," Environmental Electromagnetics, 2000. CEEM 2000. Proceedings. Asia-Pacific Conference on , vol., no., pp.232-237, 2000